A theoretical study of the stereodynamics on the abstraction reactions H/D + HS/DS*

Xu Guo-Liang(徐国亮)†, Liu Pei(刘 培), Liu Yan-Lei(刘彦磊), Liu Yu-Fang(刘玉芳), Yuan Wei(袁 伟), and Zhang Xian-Zhou(张现周)

College of Physics & Electronic Engineering, Henan Normal University, Xinxiang 453007, *China*

(Received 10 October 2012; revised manuscript received 11 December 2012)

The quasi-classical trajectory (QCT) method is employed to calculate the stereodynamics of the abstraction reactions H/D + HS/DS based on an accurate potential energy surface [Lü S J, Zhang P Y, Han K L and He G Z 2012 *J. Chem. Phys.* **136** 094308]. The reaction cross sections of the title reaction are computed, and the vector correlations for different collision energies and different initial vibrational states are presented. The influences of the collision energy and reagent vibration on the product polarization are studied, and the product polarizations of the title reactions are found to be distinctly different, which arises from the different mass factors, collision energies, and reagent vibrational states.

Keywords: quasi-classical trajectory, stereodynamics, reaction cross section, vector correlation

PACS: 82.30.Cf, 82.20.Tr, 82.20.Fd **DOI:** 10.1088/1674-1056/22/6/068203

1. Introduction

Because of its important role in combustion and atmospheric chemistry, the S + H_2 reaction and its isotopic variants have been studied both theoretically[1–9] and experimentally.[10,11] Maiti *et al.*[4] studied the intersystem crossing effect in the S + H_2 reaction by employing a "mixed" representation approach in combination with a trajectory surface-hopping method. They compared the intersystem crossing effect with that of the O + H_2 reaction. Klos *et al.*[6] reported on their theoretical study of the S(^{1}D) + H_2/D_2 →SH + H/SD + D reaction, including the nonadiabatic effect.[12] Berteloite *et al.*[7] performed kinetics and crossed-beam experiments in conditions approaching the cold energy regime, and Lee and Liu[10] investigated the S(^{1}D) + H_2 reaction and its isotopic variants through Doppler-selected time-of-flight detection of the H or D product. They determined the excitation functions and the differential cross sections at several collision energies, as well as the isotopic branching in the S(^{1}D) + HD reaction. However, little attention has been paid to the reverse reaction H + HS. In the present paper, we study the stereodynamics of the H/D + HS/DS reaction.

As is well known, the potential energy surface (PES) provides rich information about the interaction of a reactive system at a molecular level. Therefore, PES is indispensable for stereodynamics calculations. For the H + HS reaction, the first global potential energy surface was reported by Martin[13] in 1983. Then Maiti *et al.*[4] constructed the PES for the lowest triplet state of $H_2S(^3A'')$, and they studied the S + HS reaction based on the PES. Later, Klos *et al.*[6] obtained the analytical PES for $H_2S(^3A'')$ based on internally contracted multi-reference configuration interaction (MRCI) with single and double excitation levels. And recently, an accurate *ab initio* potential energy surface (PES) for the lowest triplet state of H_2S was reported by Lü *et al.*[14] On the basis of this potential energy surface, they presented an exact quantum dynamical study of the title reaction. The accurate potential energy surface makes it possible for us to study the vector properties of the reaction and its isotopic variants.

To the best of our knowledge, the vector properties of the abstraction reaction H/D + HS/DS have not been reported. Stereodynamic studies, which can provide a direct insight into the underlying chemical process from a point of view based on vector properties, have been performed in recent years. Vector properties such as the orientation and alignment of the product molecules for the A + BC→AB + C reaction were investigated in detail, and have been described in previous papers.[15–17] Combined with scalar properties, vector properties can help reveal the details of the reaction with ample space information. The major goal of the present work is thus to employ the newest PES in quasi-classical trajectory (QCT) calculations to investigate the vector correlations of the title reactions. The title reactions are as follows:

$$\begin{aligned} &H + HS \rightarrow HH + S, \quad (R1)\\ &H + DS \rightarrow HD + S, \quad (R2)\\ &D + HS \rightarrow DH + S, \quad (R3)\\ &D + DS \rightarrow DD + S. \quad (R4) \end{aligned}$$

*Project supported by the National Natural Science Foundation of China (Grant No. 11274095), the Natural Science Foundation of Henan Province, China (Grant No. 122300410109), the Natural Science Foundation of the Education Bureau of Henan Province, China (Grant No. 13A140550), the Foundation for University Yong Core Instructors of Henan Province, China (Grant No. 2009GGJS-044), and the Cultivating Fund of Henan Normal University, China (Grant No. 2010PL02).

†Corresponding author. E-mail: xugliang@htu.cn

© 2013 Chinese Physical Society and IOP Publishing Ltd

The rest of this paper is organized as follows. The QCT calculation theory is described in Section 2, while the results and discussion are given in Section 3. The major discoveries are then summarized in Section 4.

2. Theory and QCT calculations

As noted above, all the calculations performed in the present work are based on an accurate potential energy surface. The QCT method employed in this work has been described in detail elsewhere.[18–28] We focus on investigating the dynamics of the title reaction. The accuracy of the numerical integration is guaranteed by checking the conservation of the total angular momentum and the total energy for each trajectory. For each reaction, a batch of 5×10^4 trajectories is run and the integral step size is chosen to be 0.1 fs. The maximum value of the impact parameter $b_{\max}$ is computed by calculating 5×10^4 at a constant b, and sequentially increasing the b value until the reactive trajectories become one trajectory. The total reaction cross section is computed with $\sigma=\pi b_{\max}^2 N_{\rm r}/N_{\rm T}$, where $N_{\rm r}$ represents the number of reaction trajectories and $N_{\rm T}$ the total trajectories. The values of $b_{\max}$ for different collision energies are listed in Table 1.

Table 1. Values of $b_{\max}$ for the title reactions as a function of collision energy, 1 Å = 0.1 nm.

Collision energy/eV	$b_{\max}$/Å			
	H + HS	H + DS	D + HS	D + DS
0.1	1.94	1.08	0.98	0.98
0.2	2.60	2.50	2.08	2.48
0.3	2.74	2.62	2.68	2.58
0.4	2.74	2.63	2.68	2.62
0.5	2.80	2.68	2.78	2.68
0.6	2.83	2.63	2.82	2.72
0.7	2.83	2.68	2.78	2.72
0.8	2.83	2.70	2.78	2.68
1.0	2.83	2.68	2.81	2.68
1.2	2.83	2.70	2.78	2.68
1.4	2.83	2.72	2.82	2.72
1.6	2.74	2.68	2.78	2.72
1.8	2.83	2.68	2.78	2.72
2.0	2.74	2.68	2.78	2.72

The center-of-mass (CM) frame is chosen to describe the vector correlations. $\boldsymbol{k}$ and $\boldsymbol{k}'$ are the reagent relative velocity and product relative velocity, respectively. $\boldsymbol{k}$ is parallel to the z axis, and the y axis is perpendicular to the x–z plane containing the initial and final relative velocity vectors. $\theta_{\rm t}$ is the angle between $\boldsymbol{k}$ and $\boldsymbol{k}'$, which indicates the scattering direction of the product. $\boldsymbol{j}'$ is the rotational angular momentum of the product, whose polar and azimuthal angles are $\theta_{\rm r}$ and $\phi_{\rm r}$, respectively.

Four generalized polarization-dependent differential cross sections (PDDCSs) are used to describe the full three-dimensional angular distribution associated with the $\boldsymbol{k}$–$\boldsymbol{k}'$–$\boldsymbol{j}'$ correlation in the CM frame. The fully correlated CM angular distribution is written as[12,16,17,20]

$$P(\omega_{\rm t},\omega_{\rm r})=\frac{1}{2}\sum_{kq}\frac{[k]}{4\pi}\frac{1}{\sigma}\frac{{\rm d}\sigma_{kq}}{{\rm d}\omega_{\rm t}}{\rm c}_{kq}(\theta_{\rm r},\phi_{\rm r})^*, \tag{1}$$

where $[k]=2k+1, (1/\sigma)({\rm d}\sigma_{kq}/{\rm d}\omega_{\rm t})$ is the generalized polarization-dependent differential cross section,[12,21] and ${\rm c}_{kq}(\theta_{\rm r},\phi_{\rm r})$ the modified spherical harmonics.

The differential cross section is given by

$$\frac{1}{\sigma}\frac{{\rm d}\sigma_{00}}{{\rm d}\omega_{\rm t}}\equiv P(\omega_{\rm t})=\sum_{k_1}\frac{k_1}{4\pi}h_0^{k_1}(k_1,0)P_{k_1}(\cos\theta_{\rm t}). \tag{2}$$

The $P(\theta_{\rm r})$ function used to describe the k–j' correlation can be expanded in a series of Legendre polynomials[15,21] as

$$P(\theta_{\rm r})=\frac{1}{2}\sum_m(2m+1)a_0^{(m)}{\rm P}_m(\cos\theta_{\rm r}), \tag{3}$$

where

$$a_0^m=\int_0^\pi P(\theta_m){\rm P}_m(\cos\theta_{\rm r})\sin\theta_{\rm r}{\rm d}\theta_{\rm r}=\langle{\rm P}_m(\cos\theta_{\rm r})\rangle\,. \tag{4}$$

With the expanding coefficient a_0^m called the orientation (m is odd) or alignment (m is even) parameter, and the angular brackets representing an average over all the reactive trajectories. The $m=2$ value indicates the product rotational alignment, and then

$$a_0^2=\langle{\rm P}_2(\cos\theta_{\rm r})\rangle=\langle{\rm P}_2(\boldsymbol{j}'\cdot\boldsymbol{k})\rangle=\frac{1}{2}\langle3\cos^2\theta_{\rm r}-1\rangle. \tag{5}$$

The dihedral angle distribution function $P(\phi_{\rm r})$ describing the $\boldsymbol{k}$–$\boldsymbol{k}'$–$\boldsymbol{j}'$ vector correlation can be expanded into a Fourier series as[12,16]

$$P(\phi_{\rm r})=\frac{1}{2\pi}\left(1+\sum_{{\rm even},n\geq2}a_n\cos(n\phi_{\rm r})+\sum_{{\rm odd},n\geq1}b_n\sin(n\phi_{\rm r})\right), \tag{6}$$

where

$$\begin{cases}a_n=2\langle\cos(n\phi_{\rm r})\rangle\,,\\ b_n=2\langle\sin(n\phi_{\rm r})\rangle\,.\end{cases} \tag{7}$$

3. Results and discussion

As shown in Table 1, the $b_{\max}$ value for the R1 reaction is much larger than those of the other three reactions at a collision energy of 0.1 eV, and the $b_{\max}$ value for the R3 reaction is much smaller than those of the other three reactions at 0.2 eV. Obviously, the mass factor is not enough to explain the interesting phenomenon, and we guess that the structure of the intermediate product for the reaction between R1 and R3 at the lower collision energy should be taken into account. Further study is therefore necessary.

Lü *et al.*[14] computed the reaction probability of the H + HS reaction for total angular momentum $J = 0$, and found that the quantum effects have little influence on the H + HS reaction. The values of the reaction cross section σ of H + HS ($v = 0$, $j = 0$) as a function of collision energy were also calculated in Ref. [14]. We compare our result with the QM calculations from Ref. [14] as presented in Fig. 1(a). Obviously, the results of the QCT and QM methods are in good agreement with each other, which reflects the reliability of our calculations. The values of the reaction cross section σ for the title reactions are shown in Fig. 1(b). The four reaction cross sections present similar trends on the whole. With increasing collision energy, the reaction cross sections of the title reactions drop off slightly after a plateau between 0.6 eV and 1.0 eV. We attribute this behavior to the role of the translational energy, as it hinders the abstraction reactivity. It can be seen easily in Fig. 1(b) that there are distinct discrepancies between the σ of reaction R2 and the other three reactions. The reaction cross section σ of the R2 reaction is smaller than those of reactions R1, R3, and R4 for a collision energy greater than 0.4 eV. For reactions R1, R3, and R4, one can find that the differences among them are obvious in the energy range 0.2 eV–1.2 eV. Furthermore, we find that in this energy range, the reaction cross section increases with increasing mass factor. However, the discrepancies among reactions R1, R3, and R4 almost disappear when the collision energy increases to 1.2 eV or more.

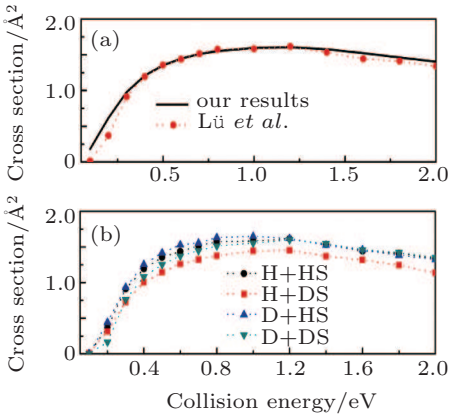


Fig. 1. (color online) (a) Comparison of the reaction cross section σ between our results and the QM calculations cited from Ref. [14]. (b) The reaction cross sections of the H + HS, H + DS, D + HS, and D + DS ($v = 0$, $j = 0$) reactions versus collision energy.

3.1. Influence of collision energy on stereodynamics

The PDDCS $(2\pi/\sigma)(\mathrm{d}\sigma_{00}/\mathrm{d}\sigma_{\omega_t})$ only describes the scattering direction or the $\boldsymbol{k}$–$\boldsymbol{k}'$ correlation of the product molecules, and has no relation to the product orientation and alignment. Figure 2 shows the $P(\theta_t)$ distributions for the four reactions, R1, R2, R3, and R4, at four different collision energies of 0.4 eV, 0.8 eV, 1.2 eV, and 1.6 eV. It is clearly proved in Fig. 2 that the peaks of the four reactions shift forward steadily with increasing collision energy. The directions of the products for the title reactions change from backwards and sideways (about 120°) to forwards and sideways (about 60°), respectively. In addition, for the title reactions, the backward scattering becomes weaker and the forward one becomes stronger when the collision energy changes from 0.4 eV to 1.6 eV. The effect of the mass factor on the scattering direction can be obtained easily when analyzing Figs. 2(a)–2(d) sequentially. The mass factor is calculated by $\cos^2\beta = m_A m_C/(m_A + m_B)(m_B + m_C)$, and the mass factors of reactions R1, R2, R3, and R4 are 0.485, 0.316, 0.646, and 0.470, respectively. Glancing over the four panels in Fig. 2, we find that the peak of $P(\theta_t)$ shifts forward with the increase in mass factor, and that the effect of the mass factor is amplified with increasing collision energy. The $P(\theta_t)$ distributions of reaction R1 and R4 show similar trends in an energy range of 0.4 eV–1.6 eV, and this may be attributed to the similar mass factors of the two reactions. It can be concluded that both the collision energy and the mass factor have an obvious influence on the $\boldsymbol{k}$–$\boldsymbol{k}'$ correlation.

Figure 3 shows the $P(\theta_r)$ distributions for the four reactions, R1, R2, R3, and R4, at four different collision energies ($E_{col} = 0.4$, 0.8, 1.2, and 1.6 eV). For the $P(\theta_r)$ distribution, it describes the $\boldsymbol{k}$–$\boldsymbol{j}'$ correlation of the product, namely the rotational alignment of the HH (HD) product. The $P(\theta_r)$ distributions, peaking at 90° and $P(\theta_r)$, are symmetrical with respect to $\theta_r = 90°$, which indicates that $\boldsymbol{j}'$ is distributed in a cylindrically symmetrical manner in the product scattering frame, and that the direction of $\boldsymbol{j}'$ is preferentially perpendicular to the $\boldsymbol{k}$ direction. Clearly, the $P(\theta_r)$ peak of reaction R3 is the lowest one, reflecting that the rotational alignment of the product for reaction R3 is the weakest. We attribute this phenomenon to the mass factor, as reaction R3 has the maximum mass factor (0.646). In Fig. 3(a), the peaks of $P(\theta_r)$ for reactions R1, R2, and R4 are all higher than that of reaction R3, and the $P(\theta_r)$ distributions of the three reactions are similar to each other. When the collision energies are 0.8 eV and 1.2 eV, it is difficult to distinguish the $P(\theta_r)$ distributions of reactions R1, R2, and R4, as shown in Figs. 3(c) and 3(d). Furthermore, from the comparison of the $P(\theta_r)$ distributions of the title reactions at four different collision energies, it is easy to see that the heights of the $P(\theta_r)$ of almost all of them are unchanged. From Fig. 3, we can conclude that the $P(\theta_r)$ distribution has a lower peak than those of the other three reactions at various collision energies, and that the rotational alignment of the product is not sensitive to collision energy.

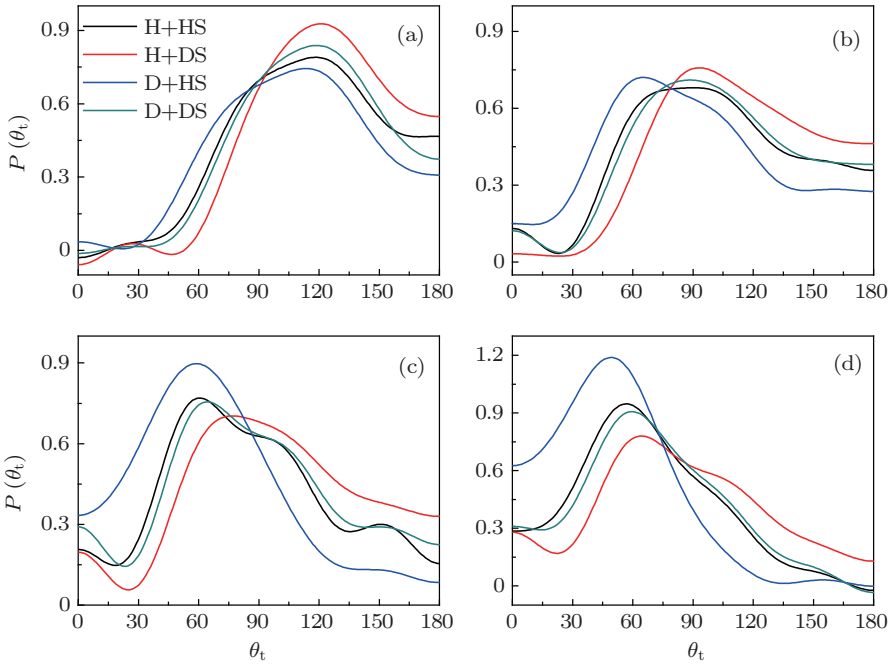


Fig. 2. (color online) The $P(\theta_t)$ distributions for the R1–R4 reactions at collision energies of 0.4 (a), 0.8 (b), 1.2 (c), and 1.6 eV (d), respectively.

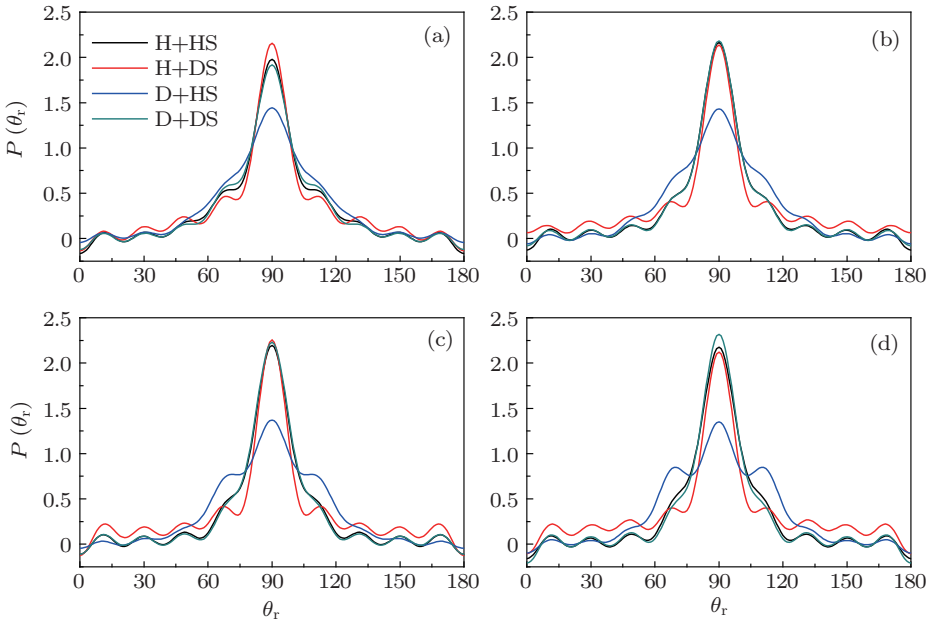


Fig. 3. (color online) The $P(\theta_r)$ distributions for the R1–R4 reactions at collision energies of 0.4 (a), 0.8 (b), 1.2 (c), and 1.6 eV (d).

The curves of the dihedral angle distribution $P(\phi_r)$ of the four reactions for the collision energies at 0.4, 0.8, 1.2, and 1.6 eV are shown in Fig. 4 and describe the $\boldsymbol{k}$–$\boldsymbol{k}'$–$\boldsymbol{j}'$ correlations. These P(ϕ_r) distributions of all four collision energies tend to be asymmetrical with respect to the $\boldsymbol{k}$–$\boldsymbol{k}'$ scattering plane (about 180°), which indicates the polarizations of angular momentum for the title reactions. The $P(\phi_r)$ distributions peak at $\phi_r = 270°$, indicating that the rotational angular momentum vectors of the products are oriented mainly along the negative y axis of the CM frame. In Fig. 4(a), the $P(\phi_r)$ distributions of the R1, R2, R3, and R4 reactions have similar trends, which means that the effect of the mass factor on the rotational orientation of the HH (HD) product is not obvious. Figures 4(b)–4(d) show the $P(\phi_r)$ distributions of the four reactions for the collision energies at 0.8, 1.2, and 1.6 eV, respectively. In Fig. 4(b), the $P(\phi_r)$ distributions are similar to those of Fig. 4(a), except that the peaks are broader and lower. Figure 4(c) shows that the peaks of $P(\phi_r)$ continue to step down. In Fig. 4(d), there are two other small peaks for the $P(\phi_r)$ distributions at about $\phi_r = 240°$ and $\phi_r = 300°$, which indicates that the rotational orientation of the product becomes weaker. In a word, the collision energy has a negative influence on the orientation of the product rotation, and the effect of the mass factor on it can be neglected for the title reactions.

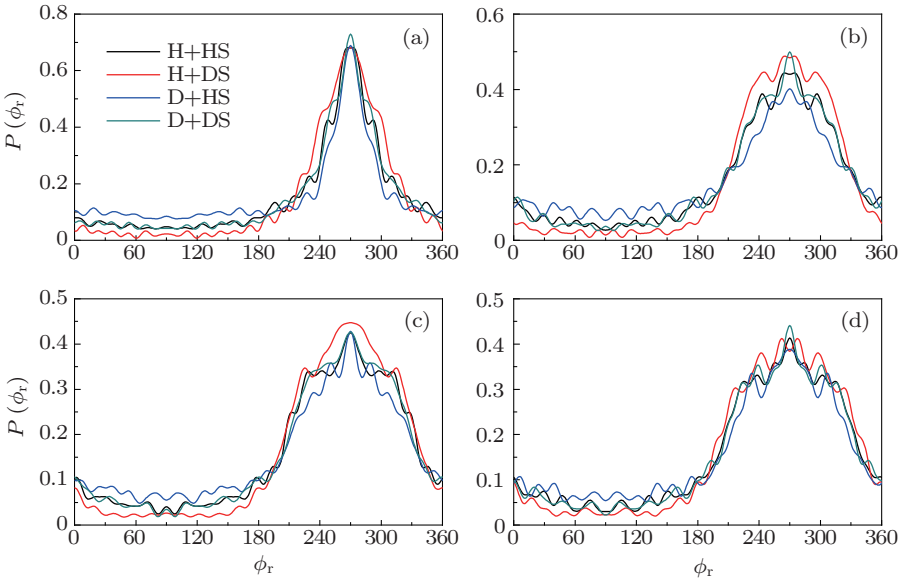


Fig. 4. (color online) The $P(\phi_r)$ distributions for the R1–R4 reactions at collision energies of 0.4 (a), 0.8 (b), 1.2 (c), and 1.6 eV (d).

3.2. Influence of reagent vibration on stereodynamics

Figures 5(a)–5(d) show the $P(\theta_t)$ distributions in three initial vibration states for the R1, R2, R3, and R4 reactions at a collision energy of 28 kcal/mole, respectively. As shown in Fig. 5(a), the products of the R1 reaction are scattered strongly sideways for $v = 0$ and $v = 1$, while the forward scattering appears to be strongest for $v = 2$. From Fig. 5(b), it can be seen clearly that the HD product prefers sideways scattering for all three initial reagent vibrations. However, the peak of $P(\theta_t)$ shifts forward slightly with increasing v. Figure 5(c) shows that the products of reaction R3 are scattered forward and sideways at $v = 0$, and they are scattered forward strongly at $v = 1$ and $v = 2$. Also, the forward scattering becomes stronger with the increase in the initial vibrational quantum number. It is clearly seen in Fig. 5(d) that the $P(\theta_t)$ distributions of the R4 reaction are similar to those of R1. Observing the four pictures in Fig. 5 carefully, we can find that the effects of the reagent vibration on the $P(\theta_t)$ distribution of the title are different from each other, which is attributed to the mass factor.

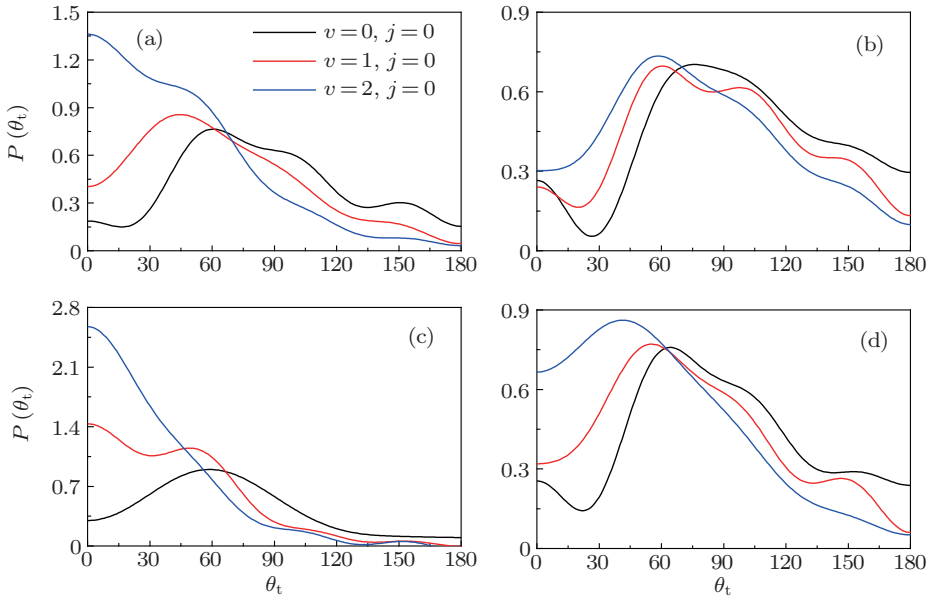


Fig. 5. (color online) Distributions of $P(\theta_t)$ at three vibrational states ($v = 0, 1, 2$, $j = 0$) for the four reactions: (a) H + HS, (b) H + DS, (c) D + HS, and (d) D + DS.

The $P(\theta_r)$ distributions at three initial vibration states for the title reactions are shown in Fig. 6. In the three initial vibrational states, the peaks of $P(\theta_r)$ of the four reactions are at $\theta_r = 90°$ and symmetrical with respect to 90°, which indicates that the $\boldsymbol{j}'$ is distributed in a cylindrically symmetrical manner in the product scattering frame and always perpendicular to $\boldsymbol{k}$.

Obviously, the peaks of the $P(\theta_r)$ distributions for the reaction are the lowest, which means the weakest rotational alignment of the products in the four reactions. This may be the result of the largest mass factor for the R3 reaction. In Fig. 6(a), the $P(\theta_r)$ distributions become broader and lower with the increase in v, reflecting that the reagent vibration has a negative influence on the alignment of the product rotation for the R1 reaction. Figure 6(b) shows that the peak of the $P(\theta_r)$ distribution for the R2 reaction at $v = 1$ is lower than that at $v = 0$, but similar to that at $v = 2$. In contrast to reaction R2, reaction R3 has a $P(\theta_r)$ distribution peak at $v = 0$, which is higher than that at $v = 1$. The $P(\theta_r)$ distributions for the R4 reaction are similar to those of R1, which can be seen in Fig. 6(d). We can then obtain the following conclusion: both the reagent vibration and mass factor influence the rotational alignment of the title reactions.

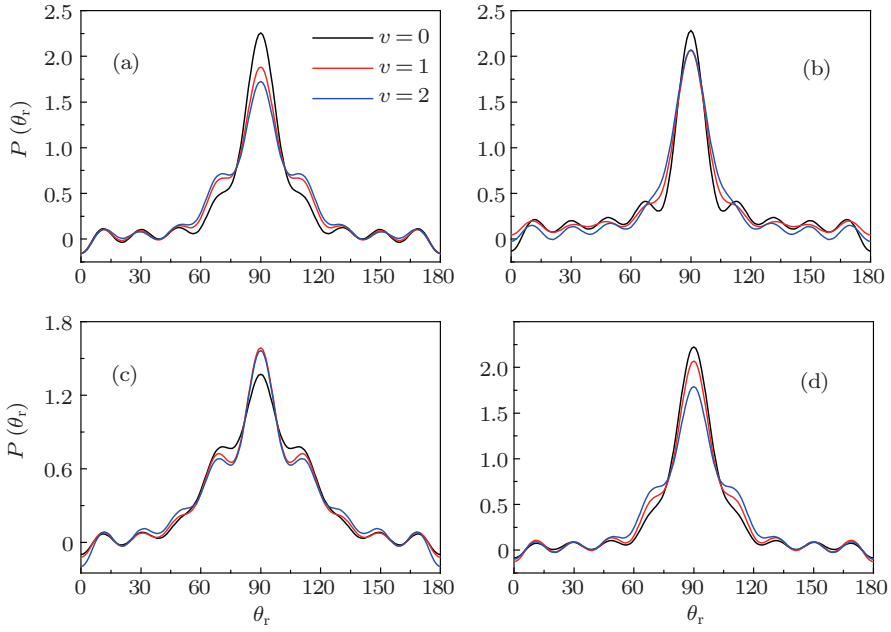


Fig. 6. (color online) Distributions of $P(\theta_r)$ in three vibrational states ($v = 0, 1, 2$, $j = 0$) for the four reactions: (a) H + HS, (b) H + DS, (c) D + HS, and (d) D + DS.

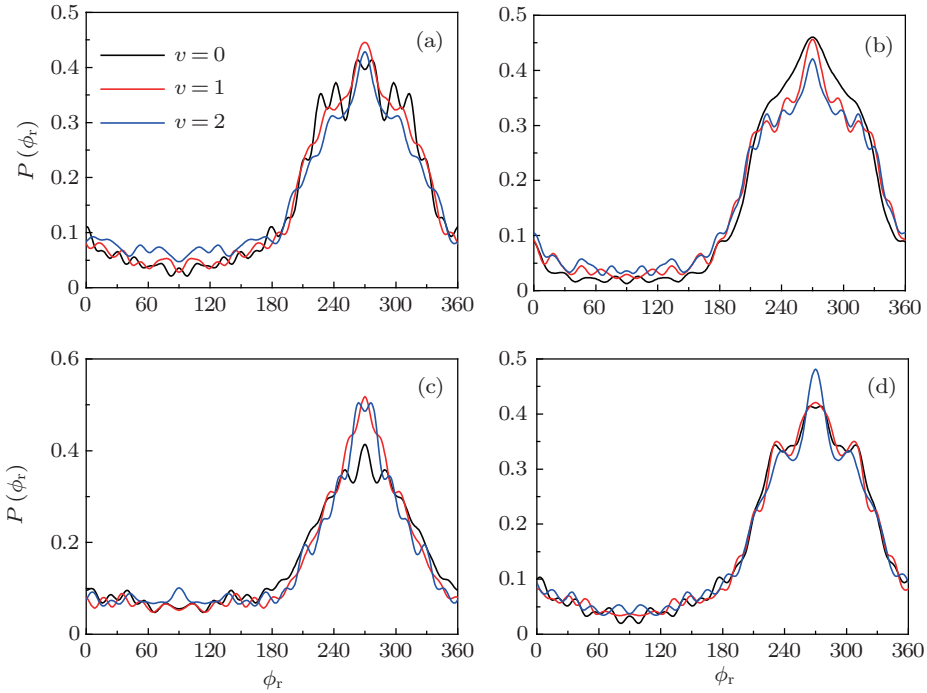


Fig. 7. (color online) Distributions of $P(\phi_r)$ at three vibrational states ($v = 0, 1, 2$, $j = 0$) for the four reactions: (a) H + HS, (b) H + DS, (c) D + HS, and (d) D + DS.

The curves of the dihedral angle distribution $P(\phi_r)$ of the four reactions in different vibrational states ($v = 0$, 1, 2) are shown in Fig. 7, and describe the $\boldsymbol{k}$–$\boldsymbol{k}'$–$\boldsymbol{j}'$ correlations. Obviously, the $P(\phi_r)$ distributions of the title reactions in three initial vibrational states are similar to those in Fig. 4. This indicates that the product rotation angular momentum vector $\boldsymbol{j}'$ is not only aligned but also oriented mainly along the negative y axis. In Fig. 7(a), the $P(\phi_r)$ distributions of the R1 reaction at $v = 0$, 1, 2 are similar to each other, indicating that the effect of reagent vibration on the orientation of the product rotation is not obvious. As shown in Fig. 7(b), the peak of $P(\phi_r)$ at $v = 2$ becomes slightly lower than at $v = 0$ and $v = 1$. The $P(\phi_r)$ of reaction R4 has a contrary trend to that of R2, as shown in Fig. 7(d). Figure 7(c) shows that the distribution of $P(\phi_r)$ at $v = 1$ is higher than that at $v = 0$, and is similar to that at $v = 2$.

In a word, both the reagent vibration and mass factor have an influence on the orientation of the product rotation, however, the influence is slight.

4. Conclusion

Stereodynamics calculations of the title reactions are performed using a QCT method based on the newest potential energy surface for the lowest triplet state of H_2S ($^3A''$). The reaction cross sections of the title reactions are calculated. The reaction cross section σ of reaction R2 is smaller than those of reactions R1, R3, and R4 for a collision energy greater than 0.4 eV, and the discrepancies among reactions R1, R3, and R4 almost disappear when the collision energy becomes greater than 1.2 eV. The $P(\theta_r)$ and $P(\phi_r)$ distributions and the PDDCS $(2\pi/\sigma)(\mathrm{d}\sigma_{00}/\mathrm{d}\sigma_{\omega_t})$ are calculated. It can be concluded that the product rotational angular momentum $\boldsymbol{j}'$ for each of the four reactions is not only aligned but also oriented mainly along the negative y axis. Furthermore, the effects of the reagent vibration and the collision on the vector correlation of the title reaction are discussed in detail. The calculations indicate that the scattering direction of products in the H + HS system is sensitive to collision energy, reagent vibration and mass factor. The $P(\theta_r)$ peak of the R3 reaction is the lowest one.

References

[1] Sengupta B S, Curtiss L and Miller J R 1996 *J. Chem. Phys.* **104** 9888
[2] Shiina H, Oya M, Yamashita K, Miyoshi A and Matsui H 1996 *J. Phys. Chem.* **100** 2136
[3] Shiina H, Miyoshi A and Matsui H 1998 *J. Chem. Phys. A* **102** 3556
[4] Maiti B, Schatz G C and Lendvay G 2004 *J. Chem. Phys. A* **108** 8772
[5] Banares L, Castillo J F, Honvault P and Launay J M 2005 *Phys. Chem. Chem. Phys.* **7** 627
[6] Kłos J A, Dagdigian P J and Alexander M H 2007 *J. Chem. Phys.* **127** 154321
[7] Berteloite C, Lara M, Bergeat A, Le Picard S D, Dayou F, Hickson K M, Canosa A, Naulin C, Launay J M, Sims I R and Costes M 2010 *Phys. Rev. Lett.* **105** 203201
[8] Lara M, Dayou F and Launay J M 2011 *Phys. Chem. Chem. Phys.* **13** 8359
[9] Lara M, Jambrina P G, Varandas A C J, Launay J M and Aoiz F 2011 *J. Chem. Phys.* **135** 134313
[10] Lee S H and Liu K 1998 *Chem. Phys. Lett.* **290** 323
[11] Lee S H and Liu K 2000 *Appl. Phys. B: Lasers* **71** 627
[12] Chen M D, Han K L and Lou N Q 2002 *Chem. Phys. Lett.* **357** 483
[13] Martin R L 1983 *Chem. Phys.* **82** 337
[14] Lü S J, Zhang P Y, Han K L and He G Z 2012 *J. Chem. Phys.* **136** 94308
[15] Han K L, He G Z and Lou N Q 1996 *J. Chem. Phys.* **105** 8699
[16] Wang M L, Han K L and He G Z 1998 *J. Chem. Phys.* **109** 5446
[17] Wang M L, Han K L and He G Z 1998 *J. Chem. Phys. A* **102** 10204
[18] Karplus M, Porter R and Sharma R 1965 *J. Chem. Phys.* **43** 3259
[19] Prisant M G, Rettner C T and Zare R N 1981 *J. Chem. Phys.* **75** 2222
[20] Shafer-Ray N E, Orr-Ewing A J and Zare R N 1995 *J. Phys. Chem.* **99** 7591
[21] Aoiz F, Brouard M and Enriquez P 1996 *J. Chem. Phys.* **105** 4964
[22] Hijazi N H and Polanyi J C 1975 *J. Chem. Phys.* **63** 2249
[23] Hijazi N H and Polanyi J C 1975 *Chem. Phys.* **11** 1
[24] Han K L, He G Z and Lou N Q 1996 *J. Chem. Phys.* **105** 8699
[25] Liu Y F, Liu Y L and Liang B 2012 *Chin. Phys. B* **21** 098201
[26] Zhao J, Xu Y and Meng Q T 2010 *Chin. Phys. B* **19** 063403
[27] Zang W, Liu Y F, Shi D H and Sun J F 2009 *Chin. Phys. B* **18** 4264
[28] Yue X F, Cheng J, Li H, Zhang Y Q and Wu E L 2010 *Chin. Phys. B* **19** 043401